Comparison of two methods for describing the strain profiles in quantum dots

C. Pryor, J. Kim, L. W. Wang, A. J. Williamson, and A. Zunger

Comparison of two methods for describing the strain profiles in quantum dots

C. Pryor
Department of Solid State Physics, Lund University, Lund, Sweden

J. Kim, L. W. Wang, A. J. Williamson, and A. Zunger[a]
National Renewable Energy Laboratory, Golden, Colorado 80401

The electronic structure of interfaces between lattice-mismatched semiconductors is sensitive to the strain. We compare two approaches for calculating such inhomogeneous strain—continuum elasticity [(CE), treated as a finite difference problem] and atomistic elasticity. While for *small* strain the two methods must agree, for the large strains that exist between lattice-mismatched III-V semiconductors (e.g., 7% for InAs/GaAs outside the linearity regime of CE) there are discrepancies. We compare the strain profile obtained by both approaches (including the approximation of the correct C_2 symmetry by the C_4 symmetry in the CE method) when applied to C_2-symmetric InAs pyramidal dots capped by GaAs. © *1998 American Institute of Physics.* [S0021-8979(98)01805-2]

I. INTRODUCTION

One of the leading methods for growing semiconductor quantum dots is via the controlled coarsening of a film of a material that is strained with respect to the substrate on which it is grown.[1,2] This (''self-assembled'') coarsening/roughening is a result of lattice-mismatch-induced strains. The dots are often capped by the substrate material, thus extending the strain around the dot to all angular directions. Not surprisingly, the interpretation of the electronic structure of such dots is profoundly affected by their strain profile. Thus, in order to calculate or interpret the measured electronic structure, one has first to calculate or measure the position dependent strain tensor $\epsilon_{\alpha\beta}$.

The three basic approaches to calculating such strains are:

(i) Harmonic continuum elasticity: Here, one uses classical elasticity[3] within the harmonic approximation. For a cubic system, the strain energy per atom, E_{CE}, is

$$E_{CE} = \frac{V}{2} C_{11}(\epsilon_{xx}^2 + \epsilon_{yy}^2 + \epsilon_{zz}^2) + \frac{V}{2} C_{44}(\epsilon_{yz}^2 + \epsilon_{zx}^2 + \epsilon_{xy}^2)$$
$$+ VC_{12}(\epsilon_{yy}\epsilon_{zz} + \epsilon_{zz}\epsilon_{xx} + \epsilon_{xx}\epsilon_{yy}), \tag{1}$$

where V is the equilibrium volume, C_{ij} are cubic elastic constants, and $\epsilon_{\alpha\beta}$ is the strain tensor. We illustrate the predictions of harmonic continuum elasticity (CE) for a two-dimensional (2D) film, since this is going to be used as a test case. In the absence of shear strain ($\epsilon_{\alpha\beta} \propto \delta_{\alpha\beta}$), for a film coherently grown on a substrate with parallel lattice constant a_s, the strain components are

$$\epsilon_{||} = \epsilon_{xx} = \epsilon_{yy} = \frac{a_s - a_{eq}}{a_{eq}}, \quad \epsilon_{\perp} = \epsilon_{zz} = \frac{c - a_{eq}}{a_{eq}}, \tag{2}$$

where a_{eq} is the equilibrium lattice constant of the unstrained material and c is the perpendicular lattice constant of the strained film. The equilibrium value of this c axis is determined from $\partial E_{CE}/\partial \epsilon_{\perp} = 0$, yielding

$$\frac{c_{eq}(a_s, \mathbf{G})}{a_{eq}} - 1 = [2 - 3q(\mathbf{G})]\epsilon_{||}(a_s), \tag{3}$$

where the ''epitaxial strain reduction factor'' for orientation $\mathbf{G}$ of the c axis is

$$q(\mathbf{G}) = 1 - \frac{B}{C_{11} + \gamma(\mathbf{G})\Delta} \tag{4}$$

and $\Delta = C_{44} - 1/2(C_{11} - C_{12})$ is the elastic anisotropy, $B = 2/3(C_{11} + 2C_{12})$ is the bulk modulus, and $\gamma(\mathbf{G})$ is a purely geometric factor given in Ref. 4. For principal directions, $\gamma(001) = 0, \gamma(011) = 1$ and $\gamma(111) = 4/3$. Equations (2)–(4) are used routinely to predict tetragonal distortions of strained films[4]. The harmonic continuum elasticity method has been recently applied to pyramidal quantum dots by Grundmann *et al.*[2] and by Pryor *et al.*[5]

(ii) Atomistic elasticity: Here one avoids a continuum description and describes the strain *energy* in terms of few-body potentials between actual atoms

$$E_{AE} = \sum_{ij} V_2(\mathbf{R}_i - \mathbf{R}_j) + \sum_{ijk} V_3(\hat{\Theta}_{ijk}) + \cdots, \tag{5}$$

where V_2 is a two-body term, and V_3 is a three-body function of the bond angle, $\hat{\Theta}_{ijk}$. The functional form of these terms is taken to be strain-independent. The strain is determined by minimizing E_{AE} with respect to atomic positions $\{\mathbf{R}\}$. Like the continuum elasticity approach, only the cubic elastic constants are used as input.[6–8] However, unlike the CE approach, here (a) optical phonon modes can be described,[6,7] (b) harmonicity is not assumed, and (c) the atomic level symmetry is retained. The last point is illustrated in Fig. 1 showing a regular pyramid representing the

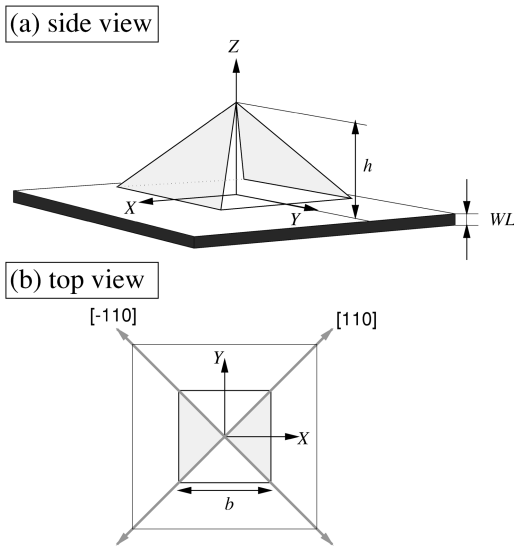[a]Electronic mail: alex_zunger@nrel.gov

     2548

FIG. 1. Schematic diagram of a square pyramidal InAs dot on (001) GaAs substrate. The wetting layer (WL) consists of 1 monolayer (ML) of In atoms. Three principal directions, $[100],[010]$ and $[001]$ are denoted as X,Y, and Z. The orientation of the pyramidal base is $X \times Y$ and the ratio of the base length (b) and the height (h) is 2 with $\{110\}$ (grey) and $\{\bar{1}10\}$ facets. Although not shown in the figure, the pyramidal InAs dot is capped by GaAs.

quantum dots from experiments of Grundmann *et al.*[2] In a continuum representation, the strain is equal on the $\{110\}$ and $\{\bar{1}10\}$ facets, while in an atomistic description these two facets can have different strain if the pyramid is made of a zincblend material. Atomistic elasticity has been widely used to determine strain in alloys,[8,9] superlattices[10] and dots,[11,12] where V_2 and V_3 of the Eq. (5) are taken from Keating's valence force field (VFF)[6–8] model.

(iii) Atomistic quantum-mechanical approach: Here one does not have to assume any model for interatomic interactions as in the atomic elasticity. Instead, one explicitly computes the total electron and nuclear energy $E_{tot}[\{\mathbf{R}_i\}]$ for each atomic configuration $\{\mathbf{R}_i\}$ directly from a quantum-mechanical Schrödinger equation. Atomic symmetry is retained and harmonicity is not assumed. This approach has been used for *small* (≤ 100 atom) wires and clusters[13,14] but it is impractical for ~ 100 Å dots ($\sim 10^5$ atoms).

The three approaches to the calculation of strain—harmonic continuum elasticity, (anharmonic) atomistic elasticity, and the atomistic quantum mechanical approached—have been recently compared for InAs/GaAs strained superlattices.[11] However, no comparison exists for 0D quantum dots. Here we perform parallel calculations for the strain $\widetilde{\epsilon}(\mathbf{R})$ of a pyramidal InAs dots (Fig. 1) surrounded by GaAs using the two approaches that are practical for large dots: continuum elasticity and atomistic elasticity. We find that: (i) The strain profiles obtained via continuum elasticity are in qualitative agreement with those found by atomistic elasticity; (ii) The atomistic elasticity produces different strains on the two facets ($\{110\}$ or $\{\bar{1}10\}$) of the zincblend pyramidal dots (see Fig. 1) corresponding to the physical c_2 symmetry, while the continuum elasticity approximates this as c_4 symmetric strain; (iii) The quantitative discrepancy resides

mostly inside the dots, while the difference in the barrier region is smaller. These differences are traced back to the fact that the strain lies outside the domain of validity for the linear elasticity. We illustrate this point by contrasting the predicted $c_{eq}(a_s,\mathbf{G})/a_{eq}$ ratio of coherent 2D films, as obtained by harmonic continuum elasticity [Eq. (3)] and atomistic elasticity (AE). Differences are noticeable already for 1% biaxial strain, whereas the controlled-coarsening (''self-assembled'') growth method for quantum dots needs to deal with larger mismatches (7% for InAs/GaAs and InP/GaP). Finally, the consequences on the electronic structure of the different strain profiles obtained for dots using CE and AE are illustrated.

II. METHODS OF CALCULATIONS

A. Continuum elasticity for dots

In the CE approximation the strain is determined by minimizing the elastic energy given in Eq. (1). To account for the lattice mismatch we assume the coordinates are fixed to the barrier material, and treat the island as expanded barrier material (with different elastic constants). This is accomplished by the modification

$$E_{CE} \rightarrow E_{CE} - \alpha(\mathbf{r})(\epsilon_{xx} + \epsilon_{yy} + \epsilon_{zz}), \tag{6}$$

$$\alpha(\mathbf{r}) = \begin{cases} 0 & \text{barrier} \\ (C_{xxxx} + 2C_{xxyy})(a_I - a_B)/a_B & \text{island} \end{cases}, \tag{7}$$

where a_B and a_I are the unstrained lattice constants for the barrier and island material, respectively, and C_{xxxx} and C_{xxyy} are the elastic constants for the island material. A piece of island material with no external forces acting on it will have its energy minimum shifted to

$$\epsilon_{ij} = \delta_{ij}(a_I - a_B)/a_B. \tag{8}$$

This fictitious strain corresponds to unstrained island material and must be subtracted. The corrected strain is still computed with derivatives in the barrier's coordinates and must be converted to the island coordinates through multiplication by dx_b/dx_I. Thus, the physical strain is given by

$$\epsilon_{ij}^{phys} = \frac{a_B}{a_I}[\epsilon_{ij} - \delta_{ij}(a_I - a_b)/a_B], \tag{9}$$

where

$$\epsilon_{ij} = \left(\frac{du_i}{dx_j} + \frac{du_j}{dx_i} \right) \Big/ 2$$

is the strain computed directly from the displacement u_i which minimizes E_{CE}.

A numerical solution requires some kind of discretization. We define the displacements u_i on a cubic grid, thereby maintaining the cubic symmetry of the crystal. The strain is expressed in terms of forwards or backwards differences by

$$\epsilon_{ij}^{\pm} = (\Delta_i^{\pm} u_j + \Delta_j^{\pm} u_i)/2, \tag{10}$$

$$\Delta_i^+ f(\mathbf{r}) = \frac{f(\mathbf{r} + \hat{\mathbf{n}}_i) - f(\mathbf{r})}{|\hat{\mathbf{n}}_i|}, \tag{11}$$

TABLE I. Ideal bond lengths (d^0), elastic constants, and force constants (α and β) of bulk GaAs and InAs. Elastic constants of valence force field method are evaluated by Eq. (8) using α and β given below.

Material	d^0_{ij} (Å)	C_{11}	C_{12}	C_{44}	α	β
		(10^{11} dyne/cm^{-1})			10^3 dyne)	
GaAs (valence force field)	2.448	12.03	5.70	5.20	41.49	8.94
GaAs (experimental)	2.448	12.11	5.48	6.04		
InAs (valence force field)	2.622	8.53	4.90	3.14	35.18	5.49
InAs (experimental)	2.622	8.329	4.526	3.959		

$$\Delta_i^- f(\mathbf{r}) = \frac{f(\mathbf{r}) - f(\mathbf{r} - \hat{\mathbf{n}}_i)}{|\hat{\mathbf{n}}_i|}, \tag{12}$$

where $\hat{\mathbf{n}}_i$ is the lattice vector in the i direction. Symmetric differences

$$\Delta_i^s f(\mathbf{r}) = \frac{f(\mathbf{r} + \hat{\mathbf{n}}_i) - f(\mathbf{r} - \hat{\mathbf{n}}_i)}{2|\hat{\mathbf{n}}_i|}, \tag{13}$$

are undesirable since they give unphysical low energy configurations which oscillate with period $2|\hat{\mathbf{n}}_i|$. For example, a displacement $u_x(\mathbf{r}) = \sin(\pi x/|\hat{\mathbf{n}}_x|)$ has $\epsilon_{xx} = 0$ when constructed using symmetric differences. The oscillatory solutions cannot be simply discarded since they mix with the physical ones. Nonsymmetric derivatives are also problematic since a particular choice will single out a direction in space. The solution is to average E_{CE} over all permutation of $\pm$ on each of the three difference operators. That is, we take $(E^{+++} + E^{-++} + E^{+-+} + \ldots)/8$. Physically this corresponds to taking the energy density at each site to be the average of the energy densities from each adjoining octant.

The elastic energy is a quadratic function of the displacements, which is easily minimized using the conjugate gradient algorithm. For the barrier material the strains are computed directly using differences (now there is no impediment to using symmetric differences). In the island material we then apply the correction in Eq. (9).

B. Atomistic valence force field for dots

In the VFF model, the strain energy is expressed as a functional of atomic positions, $\{\mathbf{R}_i\}$, as

$$E_{AE} = \sum_{ij} V_2(\mathbf{R}_i - \mathbf{R}_j) + \sum_{ijk} V_3(\hat{\theta}_{ijk})$$

$$= \frac{1}{2} \sum_i \sum_j^{nn} \frac{3\alpha_{ij}}{8(d^0_{ij})^2} [(\mathbf{R}_i - \mathbf{R}_j)^2 - (d^0_{ij})^2]^2$$

$$+ \frac{1}{2} \sum_i \sum_{j,k>j}^{nn} \frac{3\beta_{i,jk}}{8 d^0_{ij} d^0_{ij}} [(\mathbf{R}_j - \mathbf{R}_i) \times (\mathbf{R}_k - \mathbf{R}_i)$$

$$- \cos\theta_0\, d^0_{ij}\, d^0_{ij}]^2. \tag{14}$$

Here, d^0_{ij} denotes the ideal bond length between atoms i and j, and θ_0 is the ideal bond angle. For the zincblend structure, $\cos\theta_0 = -1/3$. The local-environment-dependent coefficients, α_{ij} and $\beta_{i,jk}$, are fitted to the elastic constants of bulk materials.[7] The long-range Coulomb interactions of Ref. 7

are neglected, which causes a slight deviation from the measured bulk properties.[8] In this case, the elastic constants of a pure bulk zincblend material are given as

$$C_{11} + 2C_{12} = \frac{\sqrt{3}}{4r}(3\alpha + \beta)$$

$$C_{11} - C_{12} = \frac{\sqrt{3}}{r}\beta \tag{15}$$

$$C_{44} = \frac{\sqrt{3}}{4r}\frac{4\alpha\beta}{\alpha + \beta},$$

where r is interatomic bond length. Because Eq. (15) contains only two free parameters, it is impossible to fit three arbitrary elastic constants. Nonetheless, for zincblend materials α and β may be chosen so the Cs fit within a few percent of the measured values. Table I gives the elastic constants of bulk GaAs and InAs calculated from Eq. (15) using αs and βs of Ref. 7. The elastic constants obtained differ a bit from the experimental values [since Coulomb corrections to Eq. (15) are neglected], but we will use them consistently in both our continuum elasticity and atomistic elasticity studies. For purposes of comparison, Table I also contains the experimental elastic parameters. Note that the VFF method with the standard parameterization of Eq. (15) reproduces well the values and trends in the formation enthalpies of strained GaP/InP structures, as obtained from first-principles.[15]

The relaxed atomic configuration is obtained by conjugate gradient minimization[16] of E_{AE} with respect to the atomic positions. At each minimization step, the atoms are displaced along the conjugate direction $\{\mathbf{h}\}$ by a finite increment λ, as $\mathbf{R}_i \rightarrow \mathbf{R}_i + \lambda \mathbf{h}_i$. A line minimization of E_{AE} along the conjugate gradient direction to find λ that minimizes E_{AE} is done by taking advantage of the fact that E_{AE} is a fourth-order polynomial that depends on only the relative positions, $\mathbf{R}_i - \mathbf{R}_j$, of each atom:

$$E_{AE}[\{\mathbf{R} + \lambda\mathbf{h}\}] = E_{AE}[\{\mathbf{R}_i - \mathbf{R}_j\}] + \lambda E^{(1)}[\{\mathbf{R}_i - \mathbf{R}_j\},$$

$$\times\{\mathbf{h}_i - \mathbf{h}_j\}] + \lambda^2 E^{(2)}[\{\mathbf{R}_i - \mathbf{R}_j\}, \{\mathbf{h}_i - \mathbf{h}_j\}]$$

$$+ \lambda^3 E^{(3)}[\{\mathbf{R}_i - \mathbf{R}_j\}, \{\mathbf{h}_i - \mathbf{h}_j\}]$$

$$+ \lambda^4 E^{(4)}[\{\mathbf{R}_i - \mathbf{R}_j\}, \{\mathbf{h}_i - \mathbf{h}_j\}]. \tag{16}$$

The energy terms, $E^{(1)}$, $E^{(2)}$, $E^{(3)}$, and $E^{(4)}$ are also simple
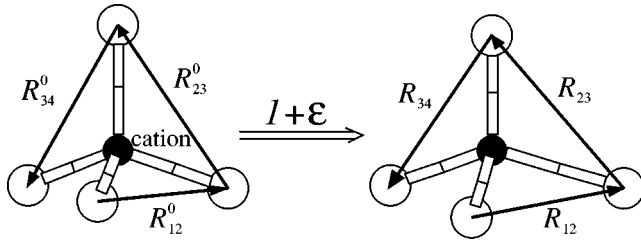
FIG. 2. Schematics to illustrate how the local strain is calculated. For a cation (Ga or In), three vectors ($\{\mathbf{R}\}$) forming a distorted tetrahedron after atomic relaxation are related to the equivalent vectors ($\{\mathbf{R}^0\}$) of an ideal tetrahedron via the strain tensor.

polynomials of $\{\mathbf{R}\}$ and $\{\mathbf{h}\}$. The increment λ minimizing the elastic energy is then obtained by solving exactly

$$\frac{\partial E_{AE}[\{\mathbf{R}+\lambda\mathbf{h}\}]}{\partial\lambda}=E^{(1)}+2\lambda E^{(2)}+3\lambda^2 E^{(3)}+4\lambda^3 E^4=0. \quad (17)$$

Figure 2 illustrates how the local strain is calculated. After the atomic positions are relaxed by minimizing E_{AE}, the local strain tensor $\widetilde{\epsilon}$ at a cation site (for cation-mixed systems) is calculated by considering a tetrahedron formed by four nearest neighboring anions. The distorted tetrahedron edges, $\mathbf{R}_{12}$, $\mathbf{R}_{23}$ and $\mathbf{R}_{34}$, are related to the ideal tetrahedron edges $\mathbf{R}_{12}^0$, $\mathbf{R}_{23}^0$ and $\mathbf{R}_{34}^0$ via

$$\begin{pmatrix} R_{12,x} & R_{23,x} & R_{34,x} \\ R_{12,y} & R_{23,y} & R_{34,y} \\ R_{12,z} & R_{23,z} & R_{34,z} \end{pmatrix}$$
$$= \begin{pmatrix} 1+\epsilon_{xx} & \epsilon_{yx} & \epsilon_{zx} \\ \epsilon_{xy} & 1+\epsilon_{yy} & \epsilon_{zy} \\ \epsilon_{xz} & \epsilon_{yz} & 1+\epsilon_{zz} \end{pmatrix}$$
$$\times \begin{pmatrix} R_{12,x}^0 & R_{23,x}^0 & R_{34,x}^0 \\ R_{12,y}^0 & R_{23,y}^0 & R_{34,y}^0 \\ R_{12,z}^0 & R_{23,z}^0 & R_{34,z}^0 \end{pmatrix}. \quad (18)$$

The ideal tetrahedron edges are $\{\mathbf{R}^0\}=\{[110]a/2,[01\bar{1}]a/2,[1\bar{1}0]a/2\}$, where a denotes the equilibrium lattice constant of the cation, i.e., a_{GaAs} for Ga atoms and a_{InAs} for In atoms. The local strain, $\widetilde{\epsilon}$, is then calculated by a matrix inversion as

$$\begin{pmatrix} \epsilon_{xx} & \epsilon_{yx} & \epsilon_{zx} \\ \epsilon_{xy} & \epsilon_{yy} & \epsilon_{zy} \\ \epsilon_{xz} & \epsilon_{yz} & \epsilon_{zz} \end{pmatrix} = \begin{pmatrix} R_{12,x} & R_{23,x} & R_{34,x} \\ R_{12,y} & R_{23,y} & R_{34,y} \\ R_{12,z} & R_{23,z} & R_{34,z} \end{pmatrix}$$
$$\times \begin{pmatrix} R_{12,x}^0 & R_{23,x}^0 & R_{34,x}^0 \\ R_{12,y}^0 & R_{23,y}^0 & R_{34,y}^0 \\ R_{12,z}^0 & R_{23,z}^0 & R_{34,z}^0 \end{pmatrix}^{-1} - I, \quad (19)$$
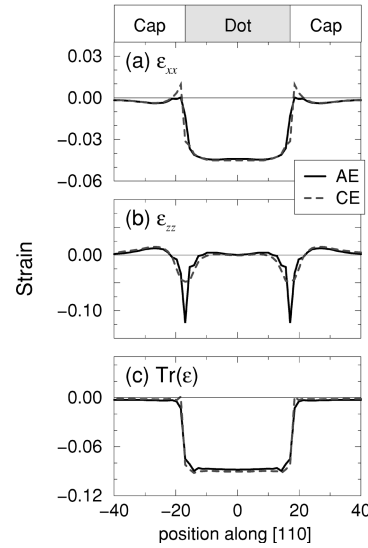
where I is the unit matrix.

FIG. 3. Strain profiles along the [110] direction at $z=h/3$ from the base of the pyramid. The solid lines are the strain profiles obtained by atomistic elasticity and dotted lines those by continuum elasticity. The positive and negative signs of X axes denote the [110] and [$\bar{1}\bar{1}0$] direction, respectively.

III. RESULTS

A. Comparison of strain profiles

Figure 3 shows ϵ_{xx}, ϵ_{zz} and $\text{Tr}(\epsilon)=\epsilon_{xx}+\epsilon_{yy}+\epsilon_{zz}$ as obtained by continuum elasticity (dashed lines) and by atomistic elasticity (solid lines) as a function of the position from the pyramidal center along the [110] direction at a height $z=h/3$ from the base (see Fig. 1). The corresponding differences in strains, $\Delta\epsilon=\epsilon(CE)-\epsilon(AE)$, are given as the solid lines in Fig. 4. We note that the grid points of the continuum elasticity calculation are chosen to be commensurate with the cation positions of the ideal GaAs zincblend structure for
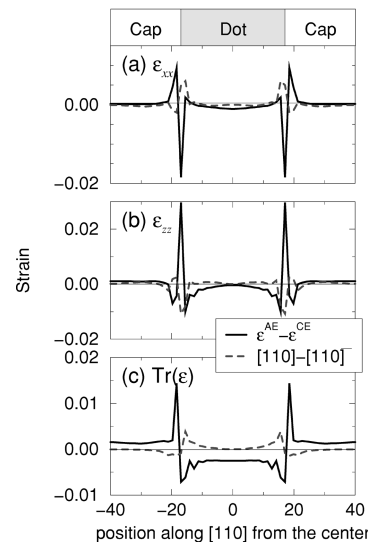

FIG. 4. Solid lines denote $\Delta\epsilon_{ij}\equiv\epsilon_{ij}(\text{CE})-\epsilon_{ij}(\text{AE})$, the difference of each strain component obtained by the continuum elasticity and the atomistic elasticity calculations. In III-V zincblend semiconductors, the [110] and [$\bar{1}10$] directions are inequivalent and, therefore, the symmetry of the pyramid is C_2. The C_2 symmetry is apparently seen by the difference of the strains (dashed lines) along the [110] and [$\bar{1}10$] directions (see Fig. 1).
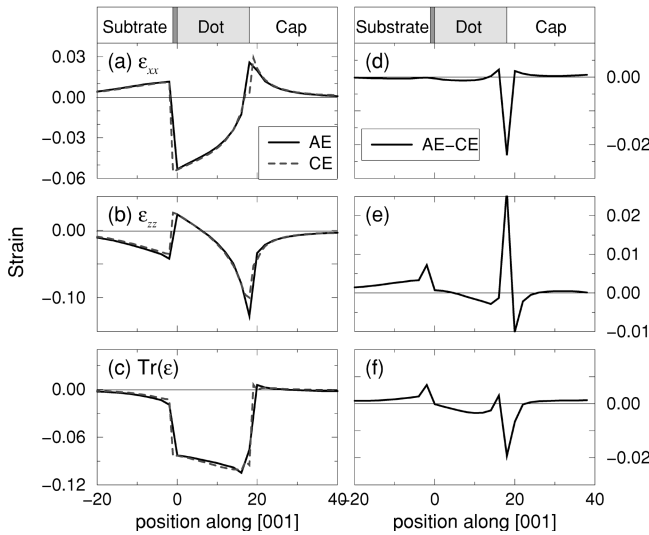
FIG. 5. Strain profiles and the differences along the Z direction through the pyramidal tip. The differences between the CE and AE are given on the right-hand side. The discrepancy is largest around the interfaces, while the strains in the barrier (GaAs substrate and capping layer) agree well within 0.5%. A significant difference is also found inside the quantum dot where the InAs experience large compressive strains at about 7% due to the lattice mismatch.
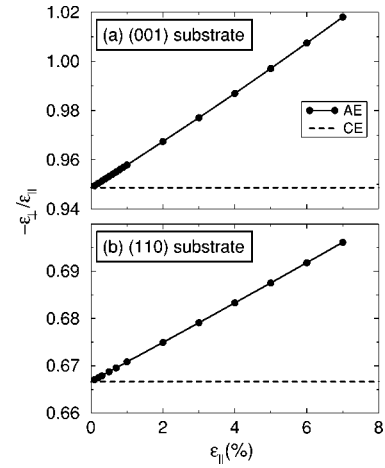

FIG. 6. Relaxation of c_{eq} of GaAs under a biaxial strain obtained by atomistic elasticity is compared to the prediction of the continuum elasticity: (a) $\mathbf{G}=[001]$ and $\epsilon_\perp/\epsilon_\parallel=-2C_{12}/C_{11}$; and (b) $\mathbf{G}=[110]$ and $\epsilon_\perp/\epsilon_\parallel=-(C_{11}+3C_{12}-2C_{44})/(C_{11}+C_{12}+2C_{44})$. At the infinitely small limit, the $-\epsilon_\perp/\epsilon_\parallel$ of the atomistic elasticity (solid lines) coincides with that of the continuum elasticity (dashed lines). The discrepancy between the CE and AE increases for the larger biaxial strains.

consistent comparisons of the two approaches. The largest differences occur around the interfaces between the dot and the cap. A significant discrepancy is also found inside the quantum dot where the InAs experiences large compressive strains: ϵ_{xx} of the continuum elasticity is found to be more compressive than that of the atomistic elasticity, while the ϵ_{zz} of the CE is more tensile. A similar comparison is given in Fig. 5, but this time the position vector is along the $Z=[001]$ direction, starting from the substrate, going through the wetting layer into the pyramidal tip and then into the capping layer. Again, the discrepancy is largest around the interfaces, while the strains in the barrier (GaAs substrate and capping layer) agree within 0.5%.

Figure 4 illustrates the extent to which the continuum elasticity description misses the correct atomic symmetry. In a pyramid made of zincblend materials on the (001) substrates, the {110} and {$\bar{1}$10} facets are symmetrically inequivalent (Fig. 1). Indeed, the atomistic calculation produces different strains. The dashed lines in Fig. 4 show the difference $\epsilon_{ij}^{AE}([110])-\epsilon_{ij}^{AE}([\bar{1}10])$ for these two directions. We see that the anisotropy is pronounced at the interfaces. For the atomistic elasticity calculation, we construct the pyramidal structure to have an In atom at the pyramidal tip. This tip In atom has: (i) two As atoms that belong to the InAs dot and lie along the [110] direction; and (ii) the other two As atoms that belong to the GaAs capping layer and lie along the [$\bar{1}$10] direction. Considering only the local strain of the tip atom, one expects larger compressive ϵ_{xx} and ϵ_{yy} along the [110] direction than along the [$\bar{1}$10] direction, based on the atomic configuration. By the same token, the atoms at the {110} interfaces experience larger compressive ϵ_{xx} and ϵ_{yy}, than those at the {$\bar{1}$10} interfaces, for this particular choice of the pyramidal geometry. In the continuum

description, $\epsilon_{ij}^{CE}([110])=\epsilon_{ij}^{CE}([\bar{1}10])$ and this effect is missing.

B. The origin of the differences—a simple test case

We know that the continuum and atomistic models, starting from the same input elastic constants, must agree in the limit of small strain and a large system. To study the rate at which the two methods diverge with increasing strain, we consider the simple case of biaxial strain. As Eqs. (2)–(4) show, for a 2-D film that is constrained on a (001) substrate, continuum elasticity predicts

$$\frac{\epsilon_\perp}{\epsilon_\parallel}\equiv\left(\frac{c-a_{eq}}{a_s-a_{eq}}\right)_{CE}=-\frac{2C_{12}}{C_{11}}. \qquad (20)$$

Figure 6(a) compares this result with that obtained via atomistic elasticity, as a function of the relative film/substrate mismatch $\epsilon_\parallel=(a_s-a_{eq})/a_{eq}$. Similarly, for the (110) strain,

$$\frac{\epsilon_\perp}{\epsilon_\parallel}=-\frac{C_{11}+3C_{12}-2C_{44}}{C_{11}+C_{12}+2C_{44}}, \qquad (21)$$

and the corresponding comparison of the continuum and atomistic elasticity is shown in Fig. 6(b). We see that the discrepancy rises linearly, reaching 4% for a lattice mismatch of 7%, characteristic of InAs/GaAs. This difference is comparable to that found between CE and AE around the interfaces of the quantum dots (Figs. 3–5). Thus, the discrepancy simply reflects the departure from the linearity regime of the continuum elasticity.

C. Consequences of the different strains in continuum elasticity and atomistic elasticity

The existence of different strain magnitudes and even symmetries in a continuum elasticity versus atomistic elasticity descriptions can affect the ensuing electronic structure

of the quantum dot. Most notably, the real point group symmetry of the square pyramid is C_2, but continuum elasticity spuriously produces a higher C_4 symmetry.

Regarding the quantitative effects, there are different levels of approximation for coupling the strain to the electronic structure. The most general and accurate electronic structure approach is atomistic (e.g., pseudopotentials, tight-binding). There, the full set of atomic positions affects the electronic structure. In more approximate electronic structure approaches, such as continuum effective mass, only some aspects of the full, position-dependent-strain tensor, $\epsilon_{ij}(\mathbf{r})$ is "felt" by the electronic structure. In these approaches, one considers strain-modified potential wells as barriers. Since experiments typically measure electronic energies rather than strains, it is instructive to examine these effects.

Assuming in decoupled conduction and valence bands the strain-modified confinement potential of the conduction-band state is

$$E_c(\mathbf{r}) = E_c^0(\mathbf{r}) + a_c(\mathbf{r})\mathrm{Tr}[\epsilon(\mathbf{r})], \qquad (22)$$

$E_c^0(\mathbf{r})$ is the energy of the conduction-band minimum of the bulk material at $\mathbf{r}$ and a_c is the deformation potential of the conduction band under hydrostatic deformation. The "strain" Hamiltonian of the valence states[17] is

$$
\begin{aligned}
H_v = a_v(\mathbf{r})\mathrm{Tr}[\epsilon(\mathbf{r})] - b\Bigg[& \begin{pmatrix} -2 & 0 & 0 \\ 0 & 1 & 0 \\ 0 & 0 & 1 \end{pmatrix}\epsilon_{xx} \\
& + \begin{pmatrix} 1 & 0 & 0 \\ 0 & -2 & 0 \\ 0 & 0 & 1 \end{pmatrix}\epsilon_{yy} + \begin{pmatrix} 1 & 0 & 0 \\ 0 & 1 & 0 \\ 0 & 0 & -2 \end{pmatrix}\epsilon_{zz} \Bigg] \\
- \sqrt{3}d\Bigg[& \begin{pmatrix} 0 & -1 & 0 \\ -1 & 0 & 0 \\ 0 & 0 & 0 \end{pmatrix}\epsilon_{xy} \\
& + \begin{pmatrix} 0 & 0 & 0 \\ 0 & 0 & -1 \\ 0 & -1 & 0 \end{pmatrix}\epsilon_{yz} + \begin{pmatrix} 0 & 0 & -1 \\ 0 & 0 & 0 \\ -1 & 0 & 0 \end{pmatrix}\epsilon_{zx} \Bigg],
\end{aligned}
$$
$$(23)$$

where a_v is the hydrostatic deformation of the valence states and b and d are uniaxial deformation potentials for (001) strain and (111) strain, respectively. The effective confinement potentials of the valence states are obtained by diagonalizing the strain Hamiltonian coupled with the spin-orbit Hamiltonian.[17] Along the [001] direction (z axis) through the pyramidal tip, the shear strains (off-diagonal terms of the strain tensor) are zero and $\epsilon_{xx} = \epsilon_{yy}$, and thus the effective confinement potentials can be simplified as

$$E_{hh} = E_v^0 + a_v\mathrm{Tr}(\epsilon) + \tfrac{1}{3}[\Delta^{so} + \Delta^s(\epsilon)] \qquad (24)$$

$$
\begin{aligned}
E_{lh} = E_v^0 &+ a_v\mathrm{Tr}(\epsilon) - \tfrac{1}{6}[\Delta^{so} + \Delta^s(\epsilon)] \\
&+ \tfrac{1}{2}\sqrt{[\Delta^{so} + \Delta^s(\epsilon)]^2 - \tfrac{8}{3}\Delta^{so}\Delta^s(\epsilon)},
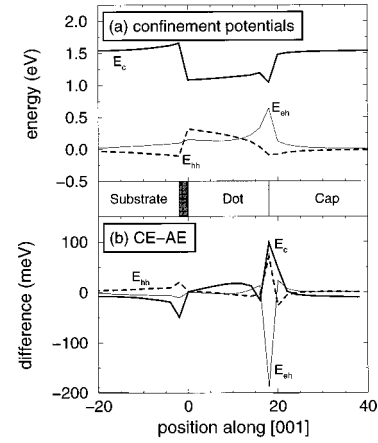\end{aligned}
$$

FIG. 7. (a) Confinement potentials by Eqs. (15) and (16), along the Z direction through the pyramidal tip in Fig. 1, predicted by the strain profiles obtained by the atomistic elasticity. All the energies are measured with respect to the valence band maximum of the bulk GaAs at equilibrium. (b) The difference of the confinement potentials by continuum elasticity and atomistic elasticity.

where Δ^{so} is the spin-orbit splitting and $\Delta^s \equiv -3b[\epsilon_{zz} - (\epsilon_{xx} + \epsilon_{yy})/2]$.

Figure 7 shows the effective confinement potentials of the conduction and valence-band states along the z axis through the tip of the pyramid. The strain profiles obtained by the continuum elasticity and atomistic elasticity are used for the calculation with the same material parameters given in Table II.[2] Again, the largest difference in confinement potentials is found at the interfaces at about 100 meV for the conduction band and 200 meV for the valence band. The average difference of the confinement potentials inside the dot is about 20 meV for the conduction-band state. Although the differences in the strain-modified-confinement potentials are small, the band edge states are expected to show different characteristics depending upon which strain profile is used for the electronic structure calculation.

IV. CONCLUSIONS

We compare the strain distribution of the pyramidal InAs dot grown on a GaAs substrate calculated using continuum elasticity and atomistic elasticity. We find a significant difference in the strain around the dot interfaces and inside the dot, while the difference in the barrier (GaAs substrate and capping layer) is very small. The difference between the two results is attributed to the large strain outside the linearity regime of CE, and to the loss of the correct atomic symmetry by the CE.

TABLE II. Material parameters used for Fig. 7.[a]

	Δ^{so}	V_v^0	a_v	b	V_c^0	a_c
GaAs	0.34	0	1.16	−1.6	1.52	−8.33
InAs	0.38	0.25	1.00	−1.8	0.66	−6.08

[a]All the numbers are given in eV from Ref. 2.

[1] W. Seifert, N. Carlsson, M. Miller, M.-E. Pistol, L. Samuelsson, and L. Wallenberg, Prog. Cryst. Growth Charact. Mater. **33**, 423 (1996).

[2] M. Grundmann, O. Stier, and D. Bimberg, Phys. Rev. B **52**, 11969 (1995).

[3] L. Landau and E. Lifshitz, *Theory of elasticity* (1959).

[4] A. Zunger, *Handbook of Crystal Growth*, edited by D. T. J. Hurle (North–Holland, Amsterdam, 1994), Vol. 3a, p. 997.

[5] C. Pryor, M.-E. Pistol, and L. Samuelson (unpublished).

[6] P. Keating, Phys. Rev. **145**, 637 (1966).

[7] R. Martin, Phys. Rev. B **1**, 4005 (1970).

[8] J. L. Martins and A. Zunger, Phys. Rev. B **30**, 6217 (1984).

[9] S.-H. Bellaiche, L. Wei, and A. Zunger, Phys. Rev. B **54**, 18568 (1996).

[10] J. Bernard and A. Zunger, Appl. Phys. Lett. **65**, 165 (1994).

[11] M. Cusack, P. Briddon, and M. Jaros, Phys. Rev. B **54**, R2300 (1996).

[12] J. Kim, L. W. Wang, and A. Zunger (unpublished).

[13] F. Buda, J. Kohanoff, and M. Parrinello, Phys. Rev. Lett. **69**, 1272 (1992).

[14] A. Saitta, F. Buda, G. Fiumara, and P. Giaquinta, Phys. Rev. B **53**, 1446 (1996).

[15] A. Silverman, A. Zunger, R. Kalish, and J. Adler, Phys. Rev. B **51**, 10795 (1995).

[16] W. H. Press, B. P. Flanner, S. A. Teukolsky, and W. T. Veteering, *Numerical Recipes* (Cambridge University Press, New York, 1989).

[17] S.-H. Wei and A. Zunger, Phys. Rev. B **49**, 14337 (1994).